Protection of p+-n Si-Photoanodes by Sputter-Deposited Ir/IrOx Thin Films

7 AUTHORS, INCLUDING:

Bastian Mei
Technical University of Denmark
30 PUBLICATIONS **240** CITATIONS

SEE PROFILE

Brian Seger
Technical University of Denmark
39 PUBLICATIONS **2,989** CITATIONS

SEE PROFILE

Thomas Pedersen
Technical University of Denmark
45 PUBLICATIONS **662** CITATIONS

SEE PROFILE

Mauro Malizia
Università della Calabria
5 PUBLICATIONS **47** CITATIONS

SEE PROFILE

# Protection of p+-n-Si Photoanodes by Sputter-Deposited Ir/IrOx Thin Films

Bastian Mei,[†] Brian Seger,[†] Thomas Pedersen,[‡] Mauro Malizia,[†] Ole Hansen,[‡] Ib Chorkendorff,[†] and Peter C. K. Vesborg*[,†]

[†]Department of Physics, CINF and [‡]Department of Micro- and Nanotechnology, Technical University of Denmark, DK-2800, Kongens Lyngby, Denmark

Ⓢ Supporting Information

ABSTRACT: Sputter deposition of Ir/IrOx on p+-n-Si without interfacial corrosion protection layers yielded photoanodes capable of efficient water oxidation (OER) in acidic media (1 M H_2SO_4). Stability of at least 18 h was shown by chronoamperometry at 1.23 V versus RHE (reversible hydrogen electrode) under 38.6 mW/cm^2 simulated sunlight irradiation ($\lambda > 635$ nm, AM 1.5G) and measurements with quartz crystal microbalances. Films exceeding a thickness of 4 nm were shown to be highly active though metastable due to an amorphous character. By contrast, 2 nm IrOx films were stable, enabling OER at a current density of 1 mA/cm^2 at 1.05 V vs. RHE. Further improvement by heat treatment resulted in a cathodic shift of 40 mV and enabled a current density of 10 mA/cm^2 (requirements for a 10% efficient tandem device) at 1.12 V vs. RHS under irradiation. Thus, the simple IrOx/Ir/p+-n-Si structures not only provide the necessary overpotential for OER at realistic device current, but also harvest ~100 mV of free energy (voltage) which makes them among the best-performing Si-based photoanodes in low-pH media.

SECTION: Energy Conversion and Storage; Energy and Charge Transport
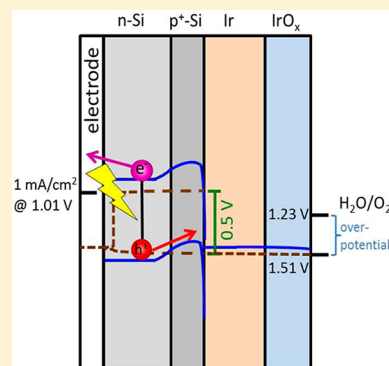
Harvesting solar light in a two-photon-driven (tandem) device is a promising strategy for the efficient generation of solar fuels such as hydrogen.[1,2] Even accounting for realistic losses due to electrochemical overpotentials and thermodynamic losses in the semiconducting absorbers, a theoretical solar to hydrogen efficiency (STH) of around 29% has been predicted.[3] Such tandem devices are widely considered to consist of a wide-band-gap photoanode coupled to a small-band-gap photocathode. Due to its band gap of 1.1 eV, Si is a good candidate for a small-band-gap material.[3] For this application, TiO_2-protected n+-p–Si photocathodes were shown to be efficient and stable devices suited for highly efficient tandem cells.[4] However, oxygen evolution is still challenging, and there is a lack of promising photoanode materials with adequate band gaps providing the required photovoltage (V_{ph}) to drive the reaction without additional bias. In a recent perspective, it was shown that the number of suitable photoanode materials and protection layers needed to fulfill all requirements of an tandem device structure is indeed rather limited.[5] Nevertheless, it may be argued that a "reversed" tandem structure, in which a large-band-gap photocathode for HER is coupled to a small-band-gap photoanode for the oxygen evolution reaction (OER), may compensate for some of the disadvantages of the (standard) tandem device structure. A major advantage of the reverse tandem design is the possibility to use metal coatings as active OER layers and protecting materials as the requirement for a transparent protecting material is lifted.

In a reversed tandem design, Si can be utilized as a small-band-gap photoanode, and progress has been made recently in protecting n-Si and p+-n-Si by various overlayers including graphene,[6] transparent conductive oxides,[7] and transition metals and their oxides[8−13] against corrosion. For example, Kenney et al.[9] evaporated a 2 nm thin Ni film on an n-Si photoanode covered by its native oxide and showed decent stability for 80 h. Nevertheless, protection was almost exclusively obtained against corrosion in alkaline media, and reports on the protection of Si photoanodes in acidic electrolyte are rare. A recent example of metal−insulator−semiconductor (MIS) junctions consisting of n-Si, thin high-quality (atomic layer deposition) TiO_2, and a thin Ir film were shown to be applicable in a wide pH range.[8] The photovoltage (V_{ph}) for these devices is in the range of 510−570 mV, and high solar to oxygen efficiencies were obtained.[8] However, an exceedingly precise control of the protecting TiO_2 layer thickness is required to achieve stability without diminishing the performance of the photoanode, for example, by tunneling resistance.[8,14] Thus, rather complex fabrication processes are needed to make this multilayer structure. In this work, we instead use OER-active materials for protective coating directly on homojunction p+-n-Si. With this simple approach, photo-

anodes can be prepared that provide photovoltages above 500 mV[4,15−17] (up to ~700 mV[16]).

Noble materials are usually required for stable electrocatalysis in acidic media, for example, to drive OER or to serve as protective coatings. Unfortunately, all known OER catalysts made from abundant elements are limited by stability to serve in neutral or basic pH.[2,18−20] It is debatable whether alkaline or acidic conditions will be favored for a commercially viable device. Therefore, stable materials for low-pH operation may be interesting.[18,21,22] Furthermore, for large-scale implementation of solar water splitting, the electrocatalytic performance is of primary importance, which is the main reason that noble metals continue to be used in the electrolysis industry.[23] Herein, we therefore report on p^+-n-Si photoanodes protected and activated by sputter-deposited Ir/IrO$_x$ thin films without using an interfacial corrosion protection layer. These photoanodes achieve a current density of 10 mA/cm^2 (~10% efficient in a tandem device) at 1.12 V versus RHE (i.e., 110 mV below the reversible potential for OER) and enable water oxidation with long-term stability in strongly acidic media (1 M H$_2$SO$_4$).

Photoanodes consisting of p^+-n Si were prepared similar to n^+-p-Si in previous reports (for further information, see the Supporting Information (SI)).[4,17] Prior to Ir/IrO$_x$ thin film deposition, the p^+-n-Si photoanode substrates were sputtered in Ar (20 mTorr, 50 sccm Ar, 35 W, for 2 min). Subsequently, a 4 nm Ir film was deposited in an Ar plasma (5 mTorr, 30 sccm Ar) at 573 K to avoid oxidation of the underlying Si. Then, IrO$_x$ was deposited by reactive sputtering of Ir in Ar/O$_2$ plasma (5 mTorr, 20 sccm Ar, 5 sccm O$_2$) at 573 K, which is known to be near the transition point between amorphous and crystalline IrO$_2$.[19,24−26] By using a calibrated sputter unit, that is, with known sputter rates, the deposited IrO$_x$ thicknesses were estimated to be 2, 4, and 6 nm, respectively. Heat treatment of the as-deposited samples was performed under vacuum (<10^{-7} mbar) at 648 and 723 K, respectively.[27] In addition to p^+-n-Si photoanode substrates, Ir/IrO$_x$ thin films were also sputter-deposited on p^+-Si materials and on Pt-coated quartz crystal microbalance (QCM) substrates. All electrochemical measurements were performed in 1 M H$_2$SO$_4$ (for further information, see the SI).

X-ray photoelectron spectroscopy revealed that the outermost layers of the as-prepared samples with different IrO$_x$ thicknesses consist of IrO$_2$ since the peak asymmetry- and binding energies of the Ir $4f_{7/2}$ lines in the range of 61.6−62.4 eV (Figure S1, SI) are well above the binding energy of metallic Ir, which is usually situated at 60.9 eV.[28,29] The slightly lower binding energy for the 2 nm thick IrO$_x$ might be due to an interaction with the underlying Ir film. This would be less pronounced with increasing film thickness. High-resolution spectra of the O 1s region (Figure 1) showed that the O 1s signal is composed of three signals that can be attributed to oxides (530.5−530.6 eV), hydroxides (531.8−532 eV), and adsorbed water (>533 eV),[28,29] thus confirming the presence of IrO$_2$-like species in all samples. Finally, depth profiling revealed that the relative thickness of the IrO$_x$ overlayer is in good agreement with the nominal thicknesses, which underscores that the composition of the O 1s is almost unchanged within the IrO$_x$ film and that a homogeneous film is obtained by sputter deposition (Figure S2, SI). Furthermore, the sputter profile evidenced a partial oxidation of the Si surface.

The electrochemical properties of these samples were recorded by cyclic voltammetry (CV) and chronoamperometry (CA) in 1 M H$_2$SO$_4$ under 38.6 mW/cm^2 of simulated sunlight
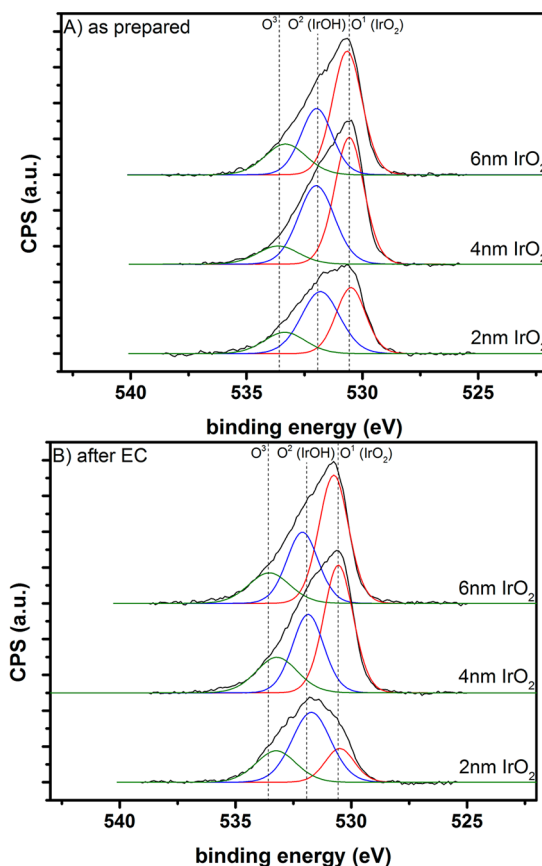
Figure 1. High-resolution XP spectra of the O 1s region for the IrO$_x$ thin films with different thicknesses. (A) The as-prepared samples and (B) samples subjected to an 18 h stability test at 1.23 V (vs RHE) in 1 M H$_2$SO$_4$ under 38.6 mW/cm^2 of simulated sunlight ($\lambda > 635$ nm, AM 1.5G).

($\lambda > 635$ nm, AM 1.5G) or in the dark. Only the red part of the spectrum was used as this material is planned to work in a "reversed" tandem device in which the blue part of the spectrum would be used by the photocathode. Representative CV scans of the as-prepared samples with different IrO$_x$ thickness are shown in Figure 2A.

The difference between the overpotentials required to obtain a current of 1 mA/cm^2 with the 4 nm IrO$_x$/Ir/p^+-Si and p^+-n Si structures (Figure 2A) measured in the dark and under irradiation reveals a photovoltage (V_{ph}) of ~500 mV (1.43−0.93 V), which is in good agreement with the V_{ph} determined for a Pt-covered p^+-n-Si (without an Ir/IrO$_x$ film) measured under dry conditions. This certainly recommends the use of the p^+-n Si photoanode since the obtained V_{ph} is already on par with good MIS junction photoanodes and there is scope for futher improvement.[8,9,16] The initial potential required to achieve a photocurrent density of 1 mA/cm^2 was found to depend on the IrO$_x$ thickness. An applied potential of 0.93 V versus RHE was measured for the thicker IrO$_x$ films (4 and 6 nm), whereas 1.05 V was required for the thin 2 nm IrO$_x$ film. The Tafel slope (Figure S3, SI) of the 2 nm thin IrO$_x$ film was measured to be 64($\pm$3) mV/dec, whereas the Tafel slopes of the thicker films were estimated to be 51($\pm$2) and 55($\pm$5) mV/dec, respectively. The saturation current density for these photoanodes was ~23 mA/cm^2 (Figure S4, SI). Furthermore, faradaic efficiencies of ~99% at 1 V versus RHE were measured for the 4 nm IrO$_x$/Ir/p^+-n-Si photoanode by oxygen

1949

dx.doi.org/10.1021/jz500865g | J. Phys. Chem. Lett. 2014, 5, 1948−1952
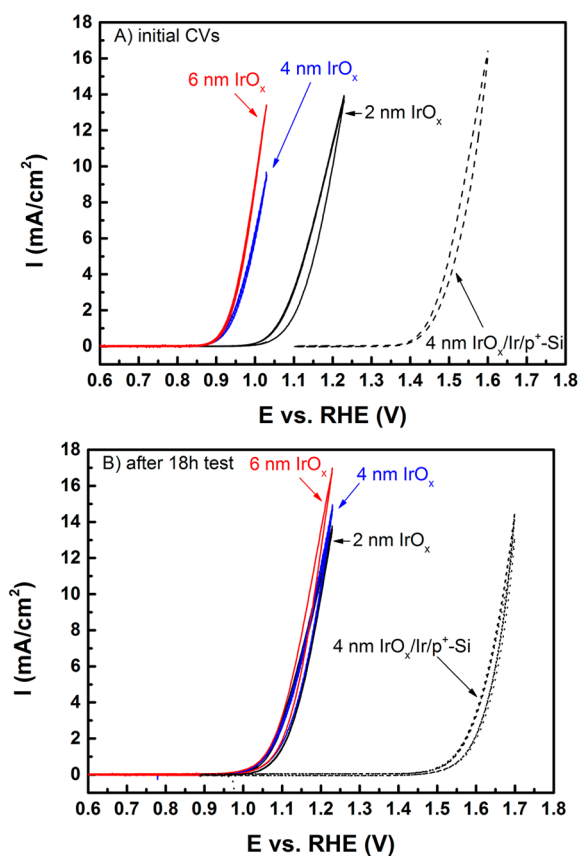
Figure 2. CV curves of the 2 (black curve), 4 (blue curve), and 6 (red curve) $IrO_x/Ir/p^+$-n-Si photoanodes measured under illumination and the 4 nm $IrO_x/Ir/p^+$-Si (black dashed line) electrode measured in the dark. (A) Initial CV scans and (B) CV scans after 18 h long-term testing at 1.23 V (vs RHE) in 1 M H_2SO_4.

quantification with gas chromatography (for further information, see the SI, Figure S5).

For the 2 nm film, the current density reaches 1 mA/cm^2 at an applied potential of 1.05 V vs. RHE and 13.8 mA/cm^2 at 1.23 V vs. RHE (potentials were not corrected for solution resistance) which resembles the performance of state-of-the-art Si photoanodes despite our lower V_{ph}.[8] For the thicker films, however, the cathodic shift of ~120 mV with increasing thickness is remarkable and clearly outperforms the state-of-the-art Si photoanodes. This may perhaps be explained with different crystallinity and porosity of the thicker films. Indeed, recent studies on amorphous and mesoporous IrO_2 show that remarkable Tafel slopes can be achieved.[29−31] In our case, it is suspected that a similar enhancement mechanism is at work for the 4 and 6 nm films, which is emphasized by XPS.

Nevertheless, CA studies performed at 1.23 V versus RHE for a total duration of 18 h indicate that the current density of all of the IrO_x thin films drops over time to stabilize at a more moderate activity. At a fixed potential of 1.23 V vs. RHE, the photocurrent of the sample with 2, 4, and 6 nm IrO_x dropped to 4.5, 4.9, and 5.5 mA/cm^2, respectively (Figure S6, SI), after which the samples appear to be stable. While this remarkable drop in current density during CA occurs within 6−10 h independent of IrO_x thickness, the associated CV shifted anodically only for the samples with 4 and 6 nm IrO_x films, almost resembling the CV curve of the 2 nm IrO_x thin film sample (Figure 2B). Curiously, allowing the electrode to sit at open circuit for some time enabled the electrodes to nearly

recover their initial CV (and high efficiency), which indicates that the high-activity state is somehow a reversible, metastable state. (Figure S7, SI).

To verify the stability of the IrO_x protection layers and the photoanode assemblies, the samples were additionally examined by XPS after a CA stability test. Furthermore, an electrochemical quartz crystal microbalance (EQCM) was prepared to determine the mass loss during long-term OER testing at 1.6 and 1.7 V versus RHE conditions. As shown in Figure 1 and Figure S1 (SI), the high-resolution XPS spectra of the O 1s and the Ir 4f region of the postelectrochemistry samples resemble the profile of the as-prepared samples. This shows that changes in the oxidation states of the IrO_x thin film due to OER within the resolution of the equipment (0.6 eV) are negligible. The EQCM data of a comparable 4 nm thick IrO_x film on a QCM substrate, which shows severe changes in the photoanode assembly during a long-term test, are shown in Figure 3.
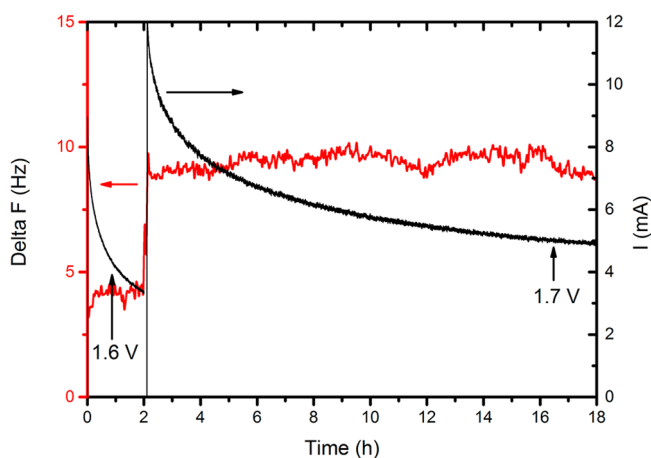
Figure 3. Current versus time behavior and changes in frequency during an 18 h long-term test of a 4 nm IrO_x thin film on a Pt-coated QCM in 1 M H_2SO_4 at 1.6 and 1.7 V versus RHE, respectively.

While the current drop during CA is similar to the drop observed for the corresponding Si-photoanode, the resonance frequency (a change of 1 Hz in resonance frequency corresponds to a mass loss of ~17 ng/cm^2) is stable during CA measurements, which clearly show that the IrO_x films do not change mass under these conditions. Subsequent CV scans up to 1.7 V versus RHE revealed that the current−potential curves are unchanged even after 18 h, and the stable resonance frequency corroborates the noncorroding nature of the electrodes (Figure S8, SI), as was already seen with XPS. Steps in frequency that are in-phase with the increase in current can be assigned to the buildup of oxygen at the electrode surface that is released during the reverse scan. Likely, the decrease in current density during testing is due to mass transport limitations of O_2 leading to a reduced effective catalytic area rather than the corrosion of the material. It has to be noted that an even more severe anodic shift of the potential was observed by Chen et al.[8] using an $Ir/TiO_2/n$-Si photoanode. They reported a drop of ~400 mV (to an applied bias of 1.5 V) to maintain a current of 1 mA at a 0.196 cm^2 electrode.

Even though the $IrO_x/Ir/p^+$-n-Si appears to be stable for at least 18 h of operation, that is, oxidation of the Si surface to SiO_2 is suppressed, the as-prepared photoanode materials were

heat-treated in vacuum at 648 and 723 K to improve the catalytic properties of the IrO_x thin films. For all heat-treated samples, activation was required, and initial repetitive potential cycling was needed until a stable CV was obtained. Among them, the 2 nm IrO_x/Ir/p$^+$-n-Si sample exhibited the most evident changes during cycling (Figure S9, SI), and the development of the current−potential curve depends strongly on heat treatment. Detailed analysis of the high-resolution O 1s region (Figure S10, SI) of the heat-treated 2 nm IrO_x/Ir/p$^+$-n-Si photoanode revealed that it is mainly the oxide component at 530.5 eV which is reduced, whereas the hydroxide component (531.8 eV) remains almost unchanged. Nevertheless, XPS shows that the oxide component redevelops during electrochemical testing via the reoxidation during initial repetitive cycling. Thus, XPS analysis confirms the reduction of the IrO_x due to heat treatment in vacuum.

The reduction of the oxide component was less pronounced for the thicker films, and CV measurement revealed that the photocurrent onset is anodically shifted with treatment temperature compared with the non-heat-treated samples (not shown). During long-term testing, the heat-treated samples of the 4 and 6 nm IrO_x thin films resembled the behavior of the as-prepared materials, that is, the CV shifted further anodically, and the current during CA dropped with time, stabilizing at ∼5 mA/cm^2 (Figure S11, SI).

Interestingly, the 2 nm IrO_x/Ir/p$^+$-n-Si behaved differently, and comparison of the stable CVs of the 2 nm IrO_x/Ir/p$^+$-n-Si sample (Figure 4A) demonstrated that the sample treated at

648 K clearly outperforms the other materials in terms of stabilized performance. Compared with the as-prepared sample, the heat-treated sample had a cathodic shift of 40 mV (at 1 mA/cm^2) and a similar Tafel slope, which results in a significant increase in current density. Thus, 10 mA/cm^2 was achieved at an applied potential of at 1.12 V versus RHE (Figure 4A). Moreover, this shift results in an improvement during long-term testing (Figure 4B). While the initial drop in current density due to mass transport was similar, an almost three times higher stable current density was obtained for the photoanode treated at 648 K. To the best of our knowledge, this is the highest photocurrent density for a Si-based photoanode in acidic electrolyte measured at 38.6 mW/cm^2 of simulated sunlight ($\lambda > 635$ nm, AM 1.5G).[8] The cathodic shift might be explained by the formation of an oxide film during reaction (XPS data) with improved catalytic performance for OER compared to the performance of the oxide film initially formed during sputtering. Moreover, we note that heat treatment might additionally lead to a more dense film and/or improved crystallinity.[25,27] Therefore, the heat-treated 2 nm IrO_x/Ir/p$^+$-n-Si photoanode demonstrates the highest stabilized photocurrent density at 1.23 V for a Si-based photoanode in an acidic electrolyte.

In conclusion, we have demonstrated that p$^+$-n-Si can be protected by sputter-deposited Ir and IrO_x thin films against corrosion during OER by means of CA, QCM, and XPS. It was shown that the IrO_x/Ir/p$^+$-n-Si photoanode assembly exhibits similar performance to the best Si-based photoanodes known. However, with increasing film thickness, a metastable phase with a much improved OER activity (1 mA/cm^2 @ 0.93 V) was obtained, but further work is required to better understand the transformation of these highly active layers during OER. Heat treatment, in particular of the photoanode with 2 nm IrO_x Ir/p$^+$-n-Si, leads to a cathodic shift of the OER onset resulting in high OER current densities at moderate potentials. Therefore, the IrO_x/Ir/p$^+$-n-Si assembly was shown to be applicable for photoelectrochemical water oxidation in acidic media. This IrO_x/Ir/p$^+$-n-Si assembly represents one of the best-performing photoanodes, and further improvement can be expected by removing the SiO_2 interlayers and using more optimized p$^+$-n-Si substrates. Due to the high iridium content of the device, the present design is not scalable to the TW level, but this work suggests the use of ultrathin dimensionally stable anode (DSA) materials instead of pure Ir/IrO_x thin films, thus substantially reducing the noble metal content. Assuming a monolayer coverage of IrO_x in such a DSA coating, the annual production of Ir (9 t/yr[32]) would (in principle) be sufficient to produce ∼0.3 TWp/yr of water splitting capacity.

Figure 4. Photoelectrochemical behavior of 2 nm IrO_x/Ir/p$^+$-n-Si subjected to different heat treatments. (A) Stabilized CV scans (potentials were not corrected for solution resistance) and (B) 18 h long-term CA tests at 1.23 V versus RHE.

■ ASSOCIATED CONTENT

ⓈSupporting Information

Experimental details, further electrochemical characterization, and characterization by XPS. This material is available free of charge via the Internet at http://pubs.acs.org.
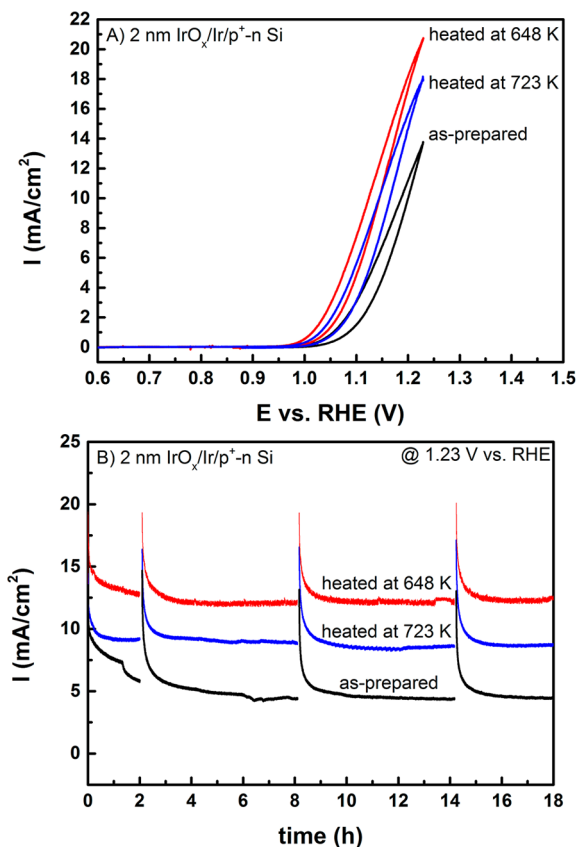
■ AUTHOR INFORMATION

Corresponding Author

*E-mail: peter.vesborg@fysik.dtu.dk.

Notes

The authors declare no competing financial interest.

■ ACKNOWLEDGMENTS

■ REFERENCES

(1) Weber, M. F.; Dignam, M. J. Efficiency of Splitting Water with Semiconducting Photoelectrodes. *Int. J. Hydrogen Energy* **1984**, *131*, 1258−1265.

(2) Walter, M. G.; Warren, E. L.; McKone, J. R.; Boettcher, S. W.; Mi, Q.; Santori, E. A; Lewis, N. S. Solar Water Splitting Cells. *Chem. Rev.* **2010**, *110*, 6446−6473.

(3) Hu, S.; Xiang, C.; Haussener, S.; Berger, A. D.; Lewis, N. S. An Analysis of the Optimal Band Gaps of Light Absorbers in Integrated Tandem Photoelectrochemical Water-Splitting Systems. *Energy Environ. Sci.* **2013**, *6*, 2984.

(4) Seger, B.; Pedersen, T.; Laursen, A. B.; Vesborg, P. C. K.; Hansen, O.; Chorkendorff, I. Using TiO_2 as a Conductive Protective Layer for Photocathodic H_2 Evolution. *J. Am. Chem. Soc.* **2013**, *135*, 1057−1064.

(5) Katsounaros, I.; Cherevko, S.; Zeradjanin, A. R.; Mayrhofer, K. J. J. Oxygen Electrochemistry as a Cornerstone for Sustainable Energy Conversion. *Angew. Chem., Int. Ed.* **2014**, *53*, 102−121.

(6) Nielander, A. C.; Bierman, M. J.; Petrone, N.; Strandwitz, N. C.; Ardo, S.; Yang, F.; Hone, J.; Lewis, N. S. Photoelectrochemical Behavior of n-Type Si(111) Electrodes Coated with a Single Layer of Graphene. *J. Am. Chem. Soc.* **2013**, *135*, 17246−17249.

(7) Sun, K.; Shen, S.; Cheung, J. S.; Pang, X.; Park, N.; Zhou, J.; Hu, Y.; Sun, Z.; Noh, S. Y.; Riley, C. T.; et al. Si Photoanode Protected by a Metal Modified ITO Layer with Ultrathin NiO_x for Solar Water Oxidation. *Phys. Chem. Chem. Phys.* **2014**, *16*, 4612−4625.

(8) Chen, Y. W.; Prange, J. D.; Dühnen, S.; Park, Y.; Gunji, M.; Chidsey, C. E. D.; McIntyre, P. C. Atomic Layer-Deposited Tunnel Oxide Stabilizes Silicon Photoanodes for Water Oxidation. *Nat. Mater.* **2011**, *10*, 539−544.

(9) Kenney, M. J.; Gong, M.; Li, Y.; Wu, J. Z.; Feng, J.; Lanza, M.; Dai, H. High-Performance Silicon Photoanodes Passivated with Ultrathin Nickel Films for Water Oxidation. *Science* **2013**, *342*, 836−840.

(10) Strandwitz, N. C.; Comstock, D. J.; Grimm, R. L.; Nichols-Nielander, A. C.; Elam, J.; Lewis, N. S. Photoelectrochemical Behavior of n-Type Si(100) Electrodes Coated with Thin Films of Manganese Oxide Grown by Atomic Layer Deposition. *J. Phys. Chem. C* **2013**, *117*, 4931−4936.

(11) Sun, K.; Park, N.; Sun, Z.; Zhou, J.; Wang, J.; Pang, X.; Shen, S.; Noh, S. Y.; Jing, Y.; Jin, S.; et al. Nickel Oxide Functionalized Silicon for Efficient Photo-Oxidation of Water. *Energy Environ. Sci.* **2012**, *5*, 7872.

(12) Sun, K.; Pang, X.; Shen, S.; Qian, X.; Cheung, J. S.; Wang, D. Metal Oxide Composite Enabled Nanotextured Si Photoanode for Efficient Solar Driven Water Oxidation. *Nano Lett.* **2013**, *13*, 2064−2072.

(13) Li, G.; Wang, S. Photoelectrochemical Characteristics of Metal-Modified Epitaxial n-Si Anodes. *J. Electroanal. Chem. Interfacial Electrochem.* **1987**, *227*, 213−221.

(14) Scheuermann, A. G.; Prange, J. D.; Gunji, M.; Chidsey, C. E. D.; McIntyre, P. C. Effects of Catalyst Material and Atomic Layer Deposited TiO_2 Oxide Thickness on the Water Oxidation Performance of Metal−Insulator−Silicon Anodes. *Energy Environ. Sci.* **2013**, *6*, 2487.

(15) Warren, E. L.; Boettcher, S. W.; Walter, M. G.; Atwater, H. A.; Lewis, N. S. pH-Independent, 520 mV Open-Circuit Voltages of Si/Methyl Viologen$^{2+/+}$ Contacts Through Use of Radial n^+p-Si Junction Microwire Array Photoelectrodes. *J. Phys. Chem. C* **2011**, *115*, 594−598.

(16) Green, M.; Emery, K.; Yoshihiro, H.; Warta, W.; Dunlop, E. D. Solar Cell Efficiency Tables (version 39). *Prog. Photovolt Res. Appl.* **2013**, *21*, 827−837.

(17) Seger, B.; Laursen, A. B.; Vesborg, P. C. K.; Pedersen, T.; Hansen, O.; Dahl, S.; Chorkendorff, I. Hydrogen Production Using a Molybdenum Sulfide Catalyst on a Titanium-Protected n^+-p-Silicon Photocathode. *Angew. Chem., Int. Ed.* **2012**, *51*, 9128−9131.

(18) Antolini, E. Iridium as Catalyst and Cocatalyst for Oxygen Evolution/reduction in Acidic Polymer Electrolyte Membrane Electrolyzers and Fuel Cells. *ACS Catal.* **2014**, *4*, 1426−1440.

(19) Spurgeon, J. M.; Velazquez, J. M.; McDowell, M. T. Improving O_2 Production of WO_3 Photoanodes with IrO_2 in Acidic Aqueous Electrolyte. *Phys. Chem. Chem. Phys.* **2014**, *16*, 3623−3631.

(20) McCrory, C. C. L.; Jung, S.; Peters, J. C.; Jaramillo, T. F. Benchmarking Heterogeneous Electrocatalysts for the Oxygen Evolution Reaction. *J. Am. Chem. Soc.* **2013**, *135*, 16977−16987.

(21) Haussener, S.; Xiang, C.; Spurgeon, J. M.; Ardo, S.; Lewis, N. S.; Weber, A. Z. Modeling, Simulation, and Design Criteria for Photoelectrochemical Water-Splitting Systems. *Energy Environ. Sci.* **2012**, *5*, 9922.

(22) McKone, J. R.; Lewis, N. S.; Gray, H. B. Will Solar-Driven Water-Splitting Devices See the Light of Day? *Chem. Mater.* **2014**, *26*, 407−414.

(23) Trasatti, S. Electrocatalysis: Understanding the Success of DSA®. *Electrochim. Acta* **2000**, *45*, 2377−2385.

(24) Hackwood, S.; Dayem, A.; Beni, G. Amorphous-Nonmetal-to-Crystalline-Metal Transition in Electrochromic Iridium Oxide Films. *Phys. Rev. B* **1982**, *26*, 471−478.

(25) Liao, P.; Chen, C.; Ho, W.; Huang, Y.; Tiong, K. Characterization of IrO_2 Thin Films by Raman Spectroscopy. *Thin Solid Films* **1997**, *301*, 7−11.

(26) Slavcheva, E.; Schnakenberg, U.; Mokwa, W. Deposition of Sputtered Iridium Oxide—Influence of Oxygen Flow in the Reactor on the Film Properties. *Appl. Surf. Sci.* **2006**, *253*, 1964−1969.

(27) Kim, H. W.; Shim, S. H.; Myung, J. H.; Lee, C. Annealing Effects on the Structural Properties of IrO_2 Thin Films. *Vacuum* **2008**, *82*, 1400−1403.

(28) Kodintsev, I. M.; Trasatti, S.; Rubel, M.; Wieckowski, A.; Kaufher, N. X-ray Photoelectron Spectroscopy and Electrochemical Surface Characterization of Iridium(IV) Oxide + Ruthenium(IV) Oxide Electrodes. *Langmuir* **1992**, *8*, 283−290.

(29) Smith, R. D. L.; Sporinova, B.; Fagan, R. D.; Trudel, S.; Berlinguette, C. P. Facile Photochemical Preparation of Amorphous Iridium Oxide Films for Water Oxidation Catalysis. *Chem. Mater.* **2014**, *26*, 1654−1659.

(30) Nakagawa, T.; Beasley, C. A.; Murray, R. W. Efficient Electro-Oxidation of Water near Its Reversible Potential by a Mesoporous IrO_x Nanoparticle Film. *J. Phys. Chem. C* **2009**, *113*, 12958−12961.

(31) Ortel, E.; Reier, T.; Strasser, P.; Kraehnert, R. Mesoporous IrO_2 Films Templated by PEO-PB-PEO Block-Copolymers: Self-Assembly, Crystallization Behavior, and Electrocatalytic Performance. *Chem. Mater.* **2011**, *23*, 3201−3209.

(32) Vesborg, P. C. K.; Jaramillo, T. F. Addressing the Terawatt Challenge: Scalability in the Supply of Chemical Elements for Renewable Energy. *RSC Adv.* **2012**, *2*, 7933.

1952

dx.doi.org/10.1021/jz500865g | *J. Phys. Chem. Lett.* 2014, 5, 1948−1952